Influence of Printed Encapsulation Layer on the Mechanical Reliability and Performance of V_2O_5 Nanowires-Based Flexible Temperature Sensors

João Neto, Abhishek Singh Dahiya, and Ravinder Dahiya, *Fellow, IEEE*

***Abstract*— Nanowires (NWs)-based sensors have been studied extensively to measure various physical, chemical, and biological parameters as their large surface-to-volume ratio leads to sensitive devices. Furthermore, due to the low flexural rigidity of NWs, these sensors can be developed on ultraflexible substrates. However, their performance often degrades after repeated mechanical deformations or when they are exposed to different ambient environments. A well-thought-out device engineering step could resolve these issues. As a potential solution, the soft material-based encapsulation layers have been explored. These are suitable for most sensor types except the temperature sensors, where they reduce the efficiency of heat transfer. Addressing this issue, we present here vanadium pentoxide (V_2O_5) NWs-based temperature sensors with nanosilica/epoxy (NS/epoxy)-based encapsulation layer. The encapsulation layer is selectively deposited with high-resolution electrohydrodynamic printing. The comparison of nonencapsulated (N-ES) and encapsulated (ES) devices, after applied mechanical loadings (bending and twisting), shows a robust and reliable temperature sensing performance of the latter. This study shows how the sensing performance can be preserved and the lifetime of flexible temperature sensors elongated by using an encapsulation layer.**

***Index Terms*— Dielectrophoresis (DEP), electronic skin (e-skin), encapsulation, flexible electronics, nanowire (NW), temperature sensor, vanadium pentoxide.**

I. Introduction

MECHANICALLY flexible or bendable physical sensors (e.g., pressure, temperature, strain, and sensors) are of significant interest in applications, such as electronic skin (e-skin) for haptic interaction [1], [2], communication and rehabilitation [3], [4], health monitoring [5], [6], the Internet of Things and robotics [7], and so on. Robust and accurate flexible sensors are needed in these applications to reliably measure various parameters of interest. However, a major issue affecting the use of many of these sensors is the degradation of their sensing performance during and/or after experiencing repeated flexing or exposure to ambient environment [8]. Factors such as humidity, bending, excessive stress during fabrication, and strain-induced during their use are responsible for the degradation of performance [8], [9]. The applications of these flexible sensors are extremely broad; ranging from very high strain applications where devices are integrated directly onto skin to applications where small but repetitive strain cycles are needed [10]. The deteriorated sensing performance is expected when the sensors are exposed to ambient environment with uncontrolled humidity [11]. Innovative solutions are needed to improve the strain tolerance and to minimize the influence of environment on the device performance.

The attempts to reduce the impact of such issues include the use of suitable flexible encapsulation layers. For example, the soft encapsulation layer has been explored for organic light-emitting diodes (OLEDs) to limit the oxygen/water permeation and enhance their lifetime to >10 000 h [12]. Furthermore, using such a protective coating, the temperature sensors with remarkable improvement in repeatability, endurance, and linearity have been reported [11]. A suitable encapsulation layer can also improve the mechanical endurance by allowing the optimal placement of various device layers in a neutral plane, which can also help prevent cracks/damage of electronic materials due to the applied mechanical stress [13], [14]. While such solution could work for most physical sensors, it is challenging to use them for temperature sensing as the encapsulation layers could reduce the efficiency of heat transfer and reduce the sensitivity, particularly when the encapsulation layer is thick.

Skin-attachable temperature sensors are needed in applications, such as health monitoring, temperature mapping during body movement, detection of covid symptoms, and so on [15], [16], [17]. Among various temperature sensitive materials investigated so far, the electrically conductive nanocomposites (NCs) containing mixture of viscoelastic polymer matrix and conductive fillers have shown most promising results [15], [18], [19], [20]. Various filler materials including carbonaceous nanomaterials (e.g., carbon nanofibers (CNFs) [18], carbon nanotubes (CNTs) [15], graphene, and reduced graphene oxide (rGO) [20], [21]), inorganic metallic nanomaterials (e.g., silver nanowires (Ag NWs) [19]), and so on have been used in the preparation of NCs for temperature sensing. These

This work was supported in part by the European commission through the NeuTouch Innovative Training Network under Grant H2020-MSCA-ITN-2018-813713, in part by the Engineering and Physical Sciences Research Council through the Engineering Fellowship for Growth under Grant EP/R029644/1, and in part by the Hetero-Print Programme under Grant EP/R03480X/1. An earlier version of this paper was presented at the 2022 IEEE International Conference on Flexible and Printable Sensors and Systems (FLEPS) [DOI: 10.1109/FLEPS53764.2022.9781483]. *(Corresponding author: Ravinder Dahiya.)*

João Neto and Abhishek Singh Dahiya are with the James Watt School of Engineering, University of Glasgow, G12 8QQ Glasgow, U.K.

Ravinder Dahiya is with the ECE Department, Northeastern University, Boston, MA 02115 USA (e-mail: r.dahiya@northeastern.edu).

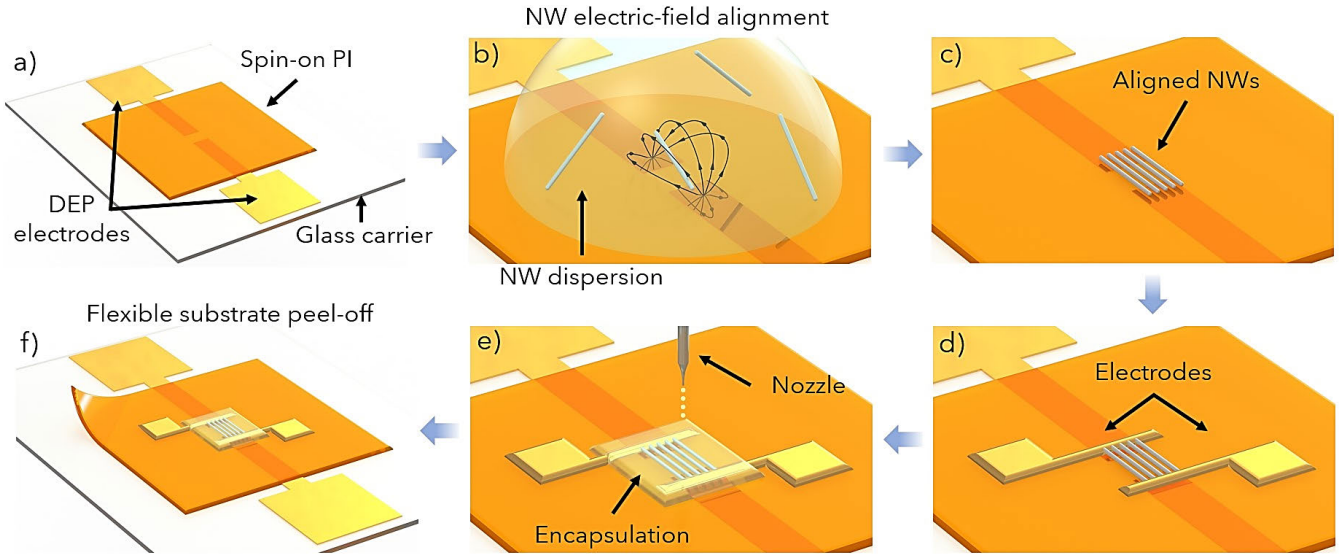

Fig. 1. Fabrication steps for V_2O_5 NWs-based flexible temperature sensor. (a) Substrate assembly containing DEP microelectrodes and spin-coated polyimide on glass carrier. (b) Electric-field alignment of drop casted NWs dispersed over the electrode gap. (c) Aligned NWs over superstrate. (d) Defined photolithography electrodes over NWs. (e) EHD printing of dielectric ink for sensor packaging. (f) Superstrate peeling-off from glass carrier.

temperature sensors have demonstrated excellent properties, such as flexibility, tunable temperature ranges, and high sensitivities. However, owing to the difficulty in controlling the dispersion state of the fillers in the polymer matrix, the NC-based temperature sensors also exhibit high thermal hysteresis and inaccuracy during cyclic heating and cooling [5]. Alternatively, inorganic metal oxides-based NWs are considered to be excellent building blocks for flexible electronics and sensing owing to their excellent characteristics, which include: 1) solution processability by having them as functional inks; 2) single crystallinity; 3) large aspect ratio for enhanced surface-to-volume ratio; and 4) excellent mechanical properties [22], [23], [24], [25], [26]. Moreover, inorganic materials are known for their stable and hysteresis free sensing response. However, external environmental factors such as relative humidity have shown to degrade their sensing performance.

To address these challenges, herein, we report V_2O_5 NWs-based robust flexible temperature sensor. This article is an extended version of the preliminary results presented at the 2022 IEEE International Conference on Flexible and Printable Sensors and Systems (FLEPS) [27]. In the initial work, was presented the dielectrophoresis (DEP) method for precise assembly of NWs at well-defined locations [28]. Next, the sensing channel was defined by following conventional photolithography, metallization, and lift-off fabrication steps. Then, the nanosilica/epoxy (NS/epoxy) layer was selectively printed, using high-resolution electrohydrodynamic (EHD) printer, to encapsulate the V_2O_5 NWs (sensing channel). Building on these preliminary results, here we present an extensive study evaluating the performance of nonencapsulated (N-ES) and encapsulated (ES) temperature sensors under similar sensing conditions (5 °C–50 °C). The data acquired using N-ES sensor showed a large change in the nominal resistance after the device substrate [i.e., polyimide (PI)] was peeled-off from the carrier glass substrate. In contrast, no such issue was observed for the ES devices, confirming the efficacy of the novel encapsulation material and its deposition method. The detailed experimental data exhibit poor stability (hysteresis and nonlinearity) for N-ES devices due to moisture and/or condensation. On the other hand, the devices with encapsulation showed stable performance.

This article is organized as follows. Section II describes the detailed experimental arrangement for alignment of NWs, device fabrication, encapsulation, and electrical characterization. Detailed temperature sensing performance for N-ES and ES devices is presented and analyzed in Section III. The key outcomes are summarized in Section IV.

II. Experimental Section

A. Nanowire Dispersion Preparation

The NW solution was prepared by dispersing 2 mg of commercially available V_2O_5 NWs (Novarials) in 10 mL of DI water. The NWs have ∼50 nm diameter and length reaching ∼1 mm. A uniform dispersion is obtained by stirring the NW solution for 30 min at 300 r/min followed by 2 min of ultrasonication to fragment the long NWs into smaller units (∼100 μm).

B. Electric-Field Assisted NW Assembly

The NW alignment process was carried out in three steps: first, the DEP microelectrode arrays (MEAs), which generate the required electric forces to attract and align NWs, were fabricated using photolithography, metal deposition, and lift-off fabrication steps. Second, a layer of PI was spin-coated on top of the MEA [Fig. 1(a)]. In the last step, a drop of NW's dispersion was casted on top of the spin-on PI substrate, and subsequently, an ac signal was applied to create the electric field and place the NWs at the desired locations [Fig. 1(b)].

The MEA was fabricated on a carrier glass slide. Before spinning the resist, carrier substrate was cleaned using the

standard procedure: a sequential 5-min ultrasonication in acetone, iso-propanol, and DI water. The carrier substrate was dried using nitrogen spray gun. The photoresist was spun and exposed to UV for development and exposed to oxygen plasma (150 W for 1 min) before metallization. The metallization process was completed by depositing 15-nm Ti and 130 nm of Au metal films through e-beam evaporation and lift-off. The DEP MEA has a 75-μm gap and 75 μm width. The gap for DEP electrodes should follow a relation, where the spacing is about 0.8 times the NW length for a maximum DEP force [29]. The PI superstrate, PI2525 from HD microsystems,[1] was spun on the fabricated DEP microelectrodes to have a thickness of $\sim$10 μm. The spinning conditions were 30 s at 500 r/min followed by 2000 r/min for a 1 min. To achieve a robust film, a second layer was spun after semi-curing the first layer at 120 °C for 2 min. Then, a hard baking step was carried out at 300 °C for 2 h. The NW assembly starts by drop casting the previously prepared NW dispersion on top of the superstrate. An ac signal is then applied to align the NWs using a signal generator WaveStation 3082 from Teledyne LeCroy and an amplifier A400DI from FLC electronics.

C. Device Fabrication and Mechanical and Electrical Characterizations

Similar photolithography process, as described above, was followed to define the temperature sensor electrodes. The defined sensing channel length/width is 16/150 μm, respectively [Fig. 1(d)]. The encapsulation was realized by printing NS/epoxy ink (from UTDots Inc.) using high-resolution EHD jet printer. Two passes (layers) of dielectric ink were printed to cover the channel zone (NWs and contact pads), as schematically shown in Fig. 1(e). The ink was cured on a hotplate for 45 min at 140 °C. Fully flexible devices on PI were obtained after dipping the carrier in water for 5 min and slowly peeling-off the spun PI substrate from one of the corners [Fig. 1(f)]. The mechanical loadings (bending and torsional) were applied using a commercial system (Yuasa System DMLHP-TW). The electrical characterizations were performed using a probe station connected to a semiconductor parameter analyser (B1500A, Agilent). The temperature sensing measurements were made by integrating a Linkam PE120 Peltier system on the probe station.

III. Results and Discussion

A. DEP Process and Device Fabrication

DEP is a versatile technique for the assembly of NWs. This method has been exclusively explored to assemble functional nanoscale electronic and photonic structures. It is an attractive low-cost technique offering precise positioning of semiconducting/metallic NWs while providing a high degree of material orientation in multidirections [30], [31]. The alignment method is based on the interactions between the nanostructure (NWs in the present case) and the solvent under an applied nonuniform electric field. The dielectrophoretic force (F_{DEP}) exerted on a high aspect-ratio oblate spheroid

[1]Trademarked.

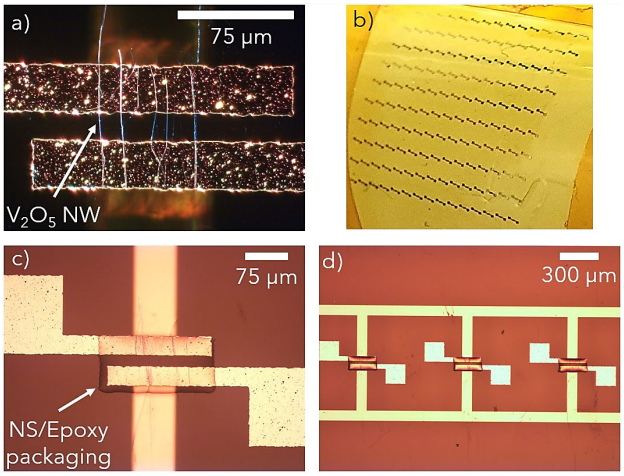

Fig. 2. Optical micrographs of the V_2O_5 NWs-based temperature sensor. (a) Dark-field image. (b) Peeled-off device without DEP microelectrodes and under bending showing high flexibility. (c) Packaged temperature sensor using NS/epoxy. (d) Array of ES temperature sensing devices.

(1-D nanomaterials) can be estimated through the following expression [28]:

$$F_{\mathrm{DEP}} = v_{\mathrm{NW}} \varepsilon_m \mathrm{Re}[K(\omega)] \nabla E^2$$

where ∇E is the gradient of the electric field, ε_m is the permittivity of the medium, v_{NW} is the volume of the NWs, and $\mathrm{Re}[K(\omega)]$ is the real part of the complex Clausius–Mossotti factor $K(\omega)$, which is dependent on the applied ac frequency.

First, a drop of NWs solution is casted on the top of the substrate assembly. The electric forces generated by the applied ac signal propagate through superstrate (PI) and reach the NW solution. Due to the electric field generated in this manner, NWs experience a dipole moment force. The torque generated by this polarization leads to the alignment of NWs according to the field lines. Simultaneously, a translation force attracts the NW toward the center of the gap, where the field is stronger due to the generated field gradient. The ac signal used here was 150 V_{PP} and 500 kHz, and the optimization steps are described in [2]. The fabricated temperature sensor is shown in Fig. 2(a) and (b), where V_2O_5 NWs can be seen bridging both sensor electrodes under dark field mode [Fig. 2(a)], resulting in a 16-μm channel. Fig. 2(c) shows the NS/epoxy ES device covering the channel region. The printed encapsulation has a thickness of $\sim$5 μm.

B. Temperature Sensing Characterizations

The influence of encapsulation layer on the mechanical reliability and stability of temperature sensor was also studied. In this regard, the performance is quantified in terms of different sensing parameters, such as sensitivity through the temperature coefficient of resistance (TCR), linearity (R^2), hysteresis (%), and nominal resistance (Ω) variation after mechanical loadings (bending and twisting). It is to note that both these sensors, i.e., ES and N-ES, are present on the same substrate. We patterned the encapsulation on one of the devices using the high-resolution drop-on-demand feature

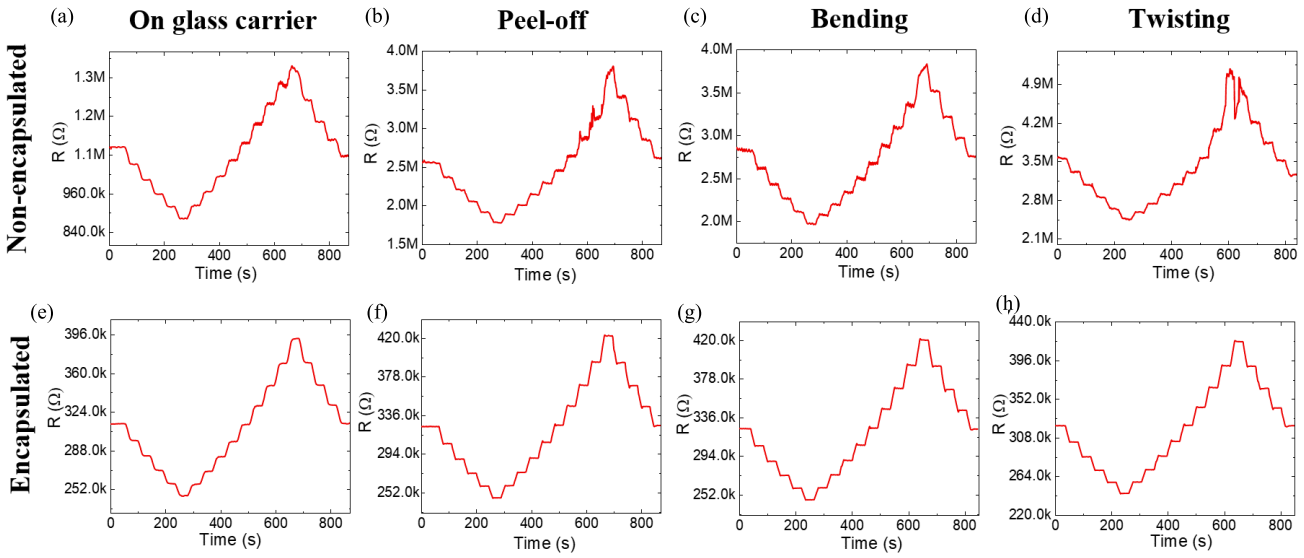

Fig. 3. Stepwise temperature sensing characterization from RT to hot (50 °C) and cold (5 °C) of ES and N-ES devices on the carrier, after peeling off and after application of mechanical stress. The resistance variation of N-ES device. (a) On glass carrier; (b) After it was peeled-off; (c) After bending; (d) After twisting. The resistance variation of encapsulated device (e) on glass carrier; (f) after peeling-off resistance; (g) after bending; and (h) after twisting.

of EHD-based jet printer. Since the devices are present on the same substrate, we characterized both sensor types under similar conditions. This also ensured a fair comparison of their performances. The performance of both N-ES and ES devices was compared in terms of these parameters obtained under the similar conditions, i.e., when they are on glass carrier, after they are peel-off (on PI substrate), and after continuous bending and twisting. For each sensor type, three devices were characterized to evaluate the repeatability.

The electrical characterizations at different temperatures were obtained by using Peltier stage while monitoring the sensor current. A bias voltage of 0.2 V was applied for these measurements. The test was conducted from room temperature (RT) (25 °C) to hot (50 °C), then to cold (5 °C), and finally returning to RT, with a 5 °C step and 30-s dwell time (time for which sensor was maintained at a constant temperature). The stepwise characterization for both device types (N-ES and ES) under different temperature conditions is shown in Fig. 3. Both device types exhibit the negative coefficient of temperature (NTC) as the resistance decreases with the increase in temperature. The increase in the conductivity of NWs with the increase in temperature is mainly due to the enhanced hopping process [32], [33]. This shows that encapsulation does not alter the mean of charge transport. However, it is to note that the ES devices showed considerably lower nominal (base) resistance. In the case of N-ES, the higher value of resistance can be attributed to the adsorption of oxygen atoms at the surface of NWs when exposed to atmosphere. Each oxygen atom is expected to trap a free electron, leading to higher resistance when compared to ES devices—which are not in contact with the ambient oxygen atoms [34]. For the ES devices, we performed thermal and plasma treatment before printing of the NS/epoxy layer to remove the adsorbed moisture from the NW surface. The encapsulation layer has restricted readsorption of the oxygen/moisture at the surface of NWs.

The TCR and linearity were extracted using the data shown in Fig. 4. The response versus temperature plots were obtained by extracting the resistance values for each temperature step shown in Fig. 3. The TCR (α) is obtained using the following equation:

$$R(T) = (R_0[1 + \alpha(T - T_0)]$$

where $R(T)$ is the resistance at temperature T and R_0 is the initial resistance tested at T_0. The extracted TCR and linearity of both sensor types is similar. The obtained TCR is $-0.96\%C^{-1}$ and $-1\%C^{-1}$ for N-EC and EC devices, where the linearity is 0.99 and 0.98, respectively.

Next, a fully functional flexible temperature sensor was obtained after peeling-off step [Fig. 2(b)]. This release process can be quite destructive because of the mismatch between the coefficient of thermal expansion (CTE) of the carrier and the spun PI. During debonding, the accumulated stress can be transferred to the device layer to generate strain on the metal electrodes and NWs [35]. Encapsulation is one approach to take care of such issues by bringing the active and electrode layers of the device closer to the neutral plane where minimum strain is observed. Fig. 3(b) and (f) shows the resulting change in resistance for both N-EC and EC devices after peeling-off. The initial resistance of N-EC device increases from 1.3Ω to 2.55 MΩ, while for the EC device, the resistance changes from 0.31Ω to 0.32 MΩ, proving that the encapsulant absorbed the released stress during the peel-off step.

The TCR increases after the sensors were peeled-off from the carrier (for both sensor types). The TCR of N-EC devices increased to $\sim 1.5\%C^{-1}$ and to $\sim 1.2\%C^{-1}$ for EC. This increase in TCR is due to the efficient heat transfer from the Peltier stage to the sensing layer after the carrier was removed. Although the sensitivity increased for both sensor type, the linearity greatly decreased for the N-EC device, from 0.99 to 0.92. When reaching cold temperatures (<10 °C), an increase in sensitivity can be observed in Fig. 3(b),

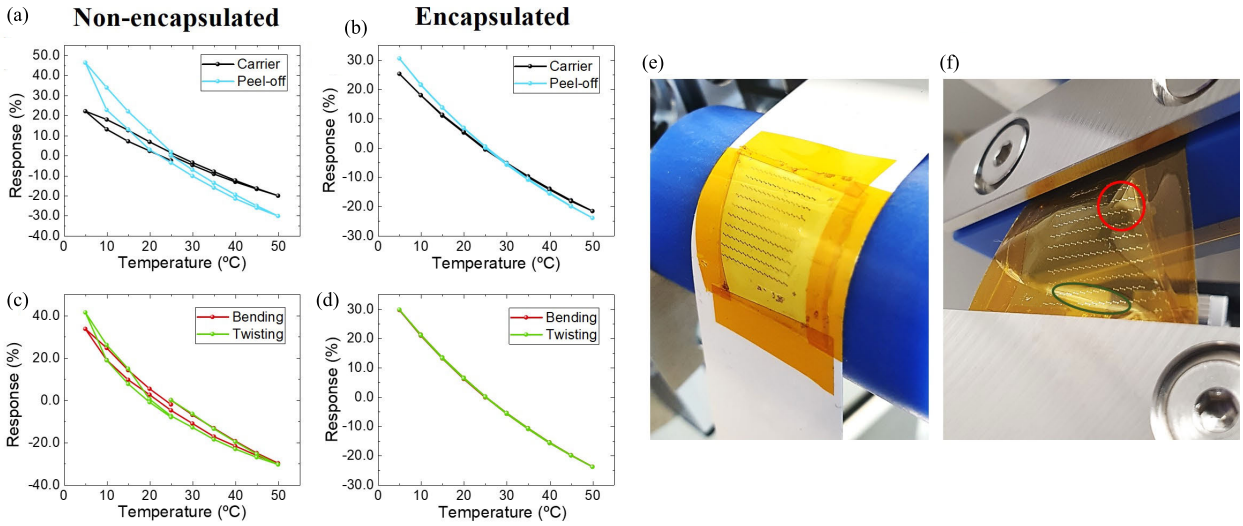

Fig. 4. Temperature response for the N-ES and ES devices for different conditions; (a) response curves between peel-off and on carrier for N-ES device; (b) response curves from both peeled and on carrier states for ES device; (c) response curves after bending and twisting of N-ES device; (d) response curves after bending and twisting for ES device; (e) sample loaded on the bending setup with 15 mm radius; (f) sample loaded on the twisting setup with 30 °C torsion, and red and green circles represent high-stress level regions according to [37].

particularly from the 10 °C to 5 °C step. This experimentally observed jump in the resistance can be explained by the charge transport in V_2O_5 through the hopping process between $V5^+$ and $V4^+$ impurity centers. It is demonstrated by the observed decline in conductivity with decreasing temperature [32]. Furthermore, with decreasing temperature, the water molecules start to condense on the NWs and the metal surface, which could also perturb the hopping process and affect the metal properties. We note that the rate of freezing increases abruptly around 5 °C, and thus, higher change in resistance was observed [36]. The precise mechanism leading to higher change in device resistance due to the adsorbed water molecules is still under consideration. Nevertheless, the cumulative effect of the abovementioned reasons leads to an increasing change in resistance at lower temperature, and therefore, a shift in sensitivity was observed. As the response of the sensor changes dynamically with the temperature, the linearity is greatly affected. On the other hand, the ES devices showed stable response and higher linearity for both cold and hot temperatures due to the highly impermeable barrier of the encapsulant.

Apart from sensitivity and linearity, it is of great importance that the sensor should recover to the initial electronic state after the temperature stimulus is removed. This is defined by the hysteresis. From Fig. 4(a) and (c), it can be observed that the N-ES sensor cannot recover to its nominal resistance at RT both from the hot and cold stimulus. The hysteresis after one cycle (i.e., from RT to hot, cold, and RT) is 1.35% on the carrier and increases to 1.75% after peel-off. On the other hand, the ES device has a negligible hysteresis of 0.3% for both on carrier and after peel-off.

C. Mechanical Reliability Characterizations

The mechanical robustness of the devices was analyzed by repeating the cyclic temperature test after applying the mechanical loadings. First, the samples were bent at a bending radius of 15 mm for 500 cycles, as shown in Fig. 4(e). Subsequently, the temperature sensing characterizations were carried out and the sample was again submitted to torsional bending by twisting it by ±30° for 500 cycles, as shown in Fig. 4(f). The extracted values are summarized in Table I.

In general, mechanical stress causes a significant degradation in performance of electronic devices based on thin films. In this work, we have used high aspect ratio V_2O_5 NWs, which offer high flexibility. However, the deposited metallic thin film electrodes are brittle, and their electrical properties could degrade after cyclic mechanical loadings. This is because the bending/twisting of sensors generates stress in the devices, which may induce the formation of cracks on the electrodes and lead to an increase in electrical resistance. During bending, the whole sample is bent along the length (parallel to NW direction), and all devices experience the same bending radius (across the entire substrate). As a result, the mechanical stress is applied uniformly to the whole substrate. However, one thing that differs from device to device in the bending test is the duration of applied bending stress, as the first-row experiences a higher bending duration (because it comes first during bending) than the following rows of devices. The tested devices were part of the third row.

The adverse effect of bending can be seen in the deviation of nominal (base) resistance of the N-ES device. It further increased after more bending and twisting cycles. Furthermore, the sensitivity and linearity of N-ES device show variations after the applied mechanical stress. The TCR got decreased to −1.3 after bending (with a linearity of ∼0.95) and to −1.5 after twisting (with a linearity of ∼0.92). The sensitivity variation after bending and twisting could be attributed to the difference of environment humidity, where precise control is required. Slight variations in humidity will affect the sensitivity especially at lower temperatures where condensation occurs. For the ES sensors, the TCR and linearity remained stable after bending and twisting mechanical loadings.

TABLE I

COMPARISON OF SENSITIVITY AND LINEARITY OF N-ES AND ES DEVICES WHILE ON CARRIER (BONDED) AND AFTER PEELING OFF FROM CARRIER (DEBONDED)

CONDITION	NON-ENCAPSULATED				ENCAPSULATED			
	TCR (%)	R^2	Hysteresis (|%|)	Nominal Resitance (MΩ)	TCR (%)	R^2	Hysteresis (|%|)	Nominal Resitance (kΩ)
Carrier	-0.96	0.99	1.35	1.1	-1	0.98	0.3	312
Peel-off	-1.5	0.92	1.75	2.56	-1.2	0.98	0.3	323
Bending	-1.3	0.95	2	2.81	-1.2	0.98	0.18	323
Twisting	-1.5	0.92	8	3.55	-1.2	0.98	0.03	321

Regarding torsion tests, it becomes more complex as the resulting stress is not uniform, and it leads to varying mechanical stress across the substrate [37]. While studying the stresses induced by our twisting setup through FEA simulation, it is found that higher stress is developed at the region close to the clamping [37] as seen in the regions defined by the red and green circles in Fig. 1. The devices presented in this study were chosen to be within that region (red circle) to test a worst case scenario, and the same devices were used throughout the study. With this, the N-ES devices clearly show the adverse effect of the torsion as the noise and high hysteresis levels were observed after twisting cycles. Furthermore, in real-life circumstances, an electronic device in applications, such as e-skin or textiles, among others, is likely to experience a combination of mechanical loadings instead of a pure bending or pure twisting loads. The developed stresses can be tensile or compressive and depend on the location of each device and many other parameters that go beyond the scope of this study.

The fatigue generated by the mechanical stress can be well observed on the hysteresis of the N-EC sensor. The bending cycles increased the hysteresis to 2%, while the strain (caused because of the applied twisting cycles) led to 8% hysteresis [Fig. 4(c)]. In Fig. 3(d), the noise level between steps is significant with partial failures at 5 °C. The considerable deterioration in stability and performance for N-ES devices could be due to the crack generation and degradation of metal–semiconductor interface. The ES devices showed no evidence of influence of the mechanical stress on the device performance as all the analyzed parameters remained constant throughout the electromechanical tests. This is due to the printed encapsulation layer that not only brings the device active and passive components closer to neutral plane by absorbing most of the stress but also ensures a robust bonding between the NW/electrode and adhesion to the flexible substrate. The other possible explanation for the observed high stability observed for ES devices is because of the pattering of the encapsulation layer. The patterning of NS/epoxy layer could significantly reduce the flexural rigidity, which results in low bending stiffness and consequently high flexibility of the ES devices.

IV. CONCLUSION

In summary, this article demonstrated the efficacy of a novel encapsulation layer and method to deposit the same on the V_2O_5 NWs-based temperature sensor. The ES devices showed robust, reliable, and more linear temperature sensing performance from 5 °C to 50 °C. The ES devices showed no change in the nominal resistance before and after peeling-off from the carrier, negligible hysteresis during a single heating-cooling cycle and high linearity as compared to N-ES sensors under similar testing conditions. The probable reasons for the observed robust and stable sensing performance of the ES devices are discussed. The present study is important for preserving the sensing performance and elongating the lifetime of the flexible temperature sensors.

ACKNOWLEDGMENT

The work in this article was initiated by R. Dahiya's Bendable Electronics and Sensing Technologies (BEST) Group when he was at University of Glasgow, Glasgow, U.K. The work got completed after he moved to Northeastern University, Boston, MA, USA, where his group is known as Bendable Electronics and Sustainable Technologies (BEST) Group.

REFERENCES

[1] R. Dahiya, D. Akinwande, and J. S. Chang, "Flexible electronic skin: From humanoids to humans," *Proc. IEEE*, vol. 107, no. 10, pp. 2011–2015, Oct. 2019, doi: 10.1109/JPROC.2019.2941665.

[2] J. Neto, R. Chirila, A. S. Dahiya, A. Christou, D. Shakthivel, and R. Dahiya, "Skin-inspired thermoreceptors-based electronic skin for biomimicking thermal pain reflexes," *Adv. Sci.*, vol. 9, no. 27, Sep. 2022, Art. no. 2201525, doi: 10.1002/advs.202201525.

[3] O. Ozioko and R. Dahiya, "Smart tactile gloves for haptic interaction, communication, and rehabilitation," *Adv. Intell. Syst.*, vol. 4, no. 2, Feb. 2022, Art. no. 2100091, doi: 10.1002/aisy.202100091.

[4] H. A. Sonar, A. P. Gerratt, S. P. Lacour, and J. Paik, "Closed-loop haptic feedback control using a self-sensing soft pneumatic actuator skin," *Soft Robot.*, vol. 7, no. 1, pp. 22–29, Feb. 2020, doi: 10.1089/soro.2019.0013.

[5] W. Jeong et al., "Accurate, hysteresis-free temperature sensor for health monitoring using a magnetic sensor and pristine polymer," *RSC Adv.*, vol. 9, no. 14, pp. 7885–7889, Mar. 2019, doi: 10.1039/C8RA10467K.

[6] F. Nikbakhtnasrabadi, E. S. Hosseini, S. Dervin, D. Shakthivel, and R. Dahiya, "Smart bandage with inductor-capacitor resonant tank based printed wireless pressure sensor on electrospun poly-*L*-lactide nanofibers," *Adv. Electron. Mater.*, vol. 8, no. 7, Jul. 2022, Art. no. 2101348, doi: 10.1002/aelm.202101348.

[7] S. Konishi and A. Hirata, "Flexible temperature sensor integrated with soft pneumatic microactuators for functional microfingers," *Sci. Rep.*, vol. 9, no. 1, p. 15634, Oct. 2019, doi: 10.1038/s41598-019-52022-x.

[8] M. Mutee ur Rehman et al., "Significance of encapsulating organic temperature sensors through spatial atmospheric atomic layer deposition for protection against humidity," *J. Mater. Sci., Mater. Electron.*, vol. 29, no. 17, pp. 14396–14405, Sep. 2018, doi: 10.1007/s10854-018-9572-4.

[9] J. Bian, L. Zhou, B. Yang, Z. Yin, and Y. Huang, "Theoretical and experimental studies of laser lift-off of nonwrinkled ultrathin polyimide film for flexible electronics," *Appl. Surf. Sci.*, vol. 499, Jan. 2020, Art. no. 143910, doi: 10.1016/j.apsusc.2019.143910.

[10] K. D. Harris, A. L. Elias, and H.-J. Chung, "Flexible electronics under strain: A review of mechanical characterization and durability enhancement strategies," *J. Mater. Sci.*, vol. 51, no. 6, pp. 2771–2805, Mar. 2016, doi: 10.1007/s10853-015-9643-3.

[11] S. W. Kim et al., "Encapsulation of polyvinyl alcohol based flexible temperature sensor through spatial atmospheric atomic layer deposition system to enhance its lifetime," *Thin Solid Films*, vol. 673, pp. 44–51, Mar. 2019, doi: 10.1016/j.tsf.2019.01.034.

[12] Z. Jia, M. B. Tucker, and T. Li, "Failure mechanics of organic–inorganic multilayer permeation barriers in flexible electronics," *Compos. Sci. Technol.*, vol. 71, no. 3, pp. 365–372, Feb. 2011, doi: 10.1016/j.compscitech.2010.12.003.

[13] A. Vilouras, A. Christou, L. Manjakkal, and R. Dahiya, "Ultrathin ion-sensitive field-effect transistor chips with bending-induced performance enhancement," *ACS Appl. Electron. Mater.*, vol. 2, no. 8, pp. 2601–2610, Aug. 2020, doi: 10.1021/acsaelm.0c00489.

[14] J. A. Rogers, T. Someya, and Y. Huang, "Materials and mechanics for stretchable electronics," *Science*, vol. 327, no. 5973, pp. 1603–1607, Mar. 2013, doi: doi:10.1126/science.1182383.

[15] Y. Kumaresan, O. Ozioko, and R. Dahiya, "Multifunctional electronic skin with a stack of temperature and pressure sensor arrays," *IEEE Sensors J.*, vol. 21, no. 23, pp. 26243–26251, Dec. 2021, doi: 10.1109/JSEN.2021.3055458.

[16] J. Shin et al., "Sensitive wearable temperature sensor with seamless monolithic integration," *Adv. Mater.*, vol. 32, no. 2, Jan. 2020, Art. no. 1905527, doi: 10.1002/adma.201905527.

[17] S. Y. Hong et al., "Stretchable active matrix temperature sensor array of polyaniline nanofibers for electronic skin," *Adv. Mater.*, vol. 28, no. 5, pp. 930–935, Feb. 2016, doi: 10.1002/adma.201504659.

[18] J.-H. Lee et al., "Flexible temperature sensors made of aligned electrospun carbon nanofiber films with outstanding sensitivity and selectivity towards temperature," *Mater. Horizons*, vol. 8, no. 5, pp. 1488–1498, May 2021, doi: 10.1039/d1mh00018g.

[19] Z. Cui, F. R. Poblete, and Y. Zhu, "Tailoring the temperature coefficient of resistance of silver nanowire nanocomposites and their application as stretchable temperature sensors," *ACS Appl. Mater. Interfaces*, vol. 11, no. 19, pp. 17836–17842, May 2019, doi: 10.1021/acsami.9b04045.

[20] T. Q. Trung, S. Ramasundaram, B.-U. Hwang, and N.-E. Lee, "An all-elastomeric transparent and stretchable temperature sensor for body-attachable wearable electronics," *Adv. Mater.*, vol. 28, no. 3, pp. 502–509, 2016, doi: 10.1002/adma.201504441.

[21] L. Dan and A. L. Elias, "Flexible and stretchable temperature sensors fabricated using solution-processable conductive polymer composites," *Adv. Healthcare Mater.*, vol. 9, no. 16, Aug. 2020, Art. no. 2000380, doi: 10.1002/adhm.202000380.

[22] W. Taube Navaraj et al., "Nanowire FET based neural element for robotic tactile sensing skin," *Frontiers Neurosci.*, vol. 11, Sep. 2017, Art. no. 501, doi: 10.3389/fnins.2017.00501.

[23] D. Shakthivel, A. S. Dahiya, R. Mukherjee, and R. Dahiya, "Inorganic semiconducting nanowires for green energy solutions," *Current Opinion Chem. Eng.*, vol. 34, Dec. 2021, Art. no. 100753, doi: 10.1016/j.coche.2021.100753.

[24] A. S. Dahiya, A. Christou, J. Neto, A. Zumeit, D. Shakthivel, and R. Dahiya, "In tandem contact-transfer printing for high-performance transient electronics," *Adv. Electron. Mater.*, vol. 8, no. 9, Sep. 2022, Art. no. 2200170, doi: 10.1002/aelm.202200170.

[25] Y. Kumaresan, S. Ma, O. Ozioko, and R. Dahiya, "Soft capacitive pressure sensor with enhanced sensitivity assisted by ZnO NW interlayers and airgap," *IEEE Sensors J.*, vol. 22, no. 5, pp. 3974–3982, Mar. 2022, doi: 10.1109/JSEN.2022.3143030.

[26] A. S. Dahiya, D. Shakthivel, Y. Kumaresan, A. Zumeit, A. Christou, and R. Dahiya, "High-performance printed electronics based on inorganic semiconducting nano to chip scale structures," *Nano Converg.*, vol. 7, no. 1, p. 33, Dec. 2020, doi: 10.1186/s40580-020-00243-6.

[27] J. Neto, A. S. Dahiya, and R. Dahiya, "Influence of encapsulation on the performance of V_2O_5 nanowires-based temperature sensors," in *Proc. IEEE Int. Conf. Flexible Printable Sensors Syst. (FLEPS)*, Jul. 2022, pp. 1–4, doi: 10.1109/FLEPS53764.2022.9781483.

[28] S. Raychaudhuri, S. A. Dayeh, D. Wang, and E. T. Yu, "Precise semiconductor nanowire placement through dielectrophoresis," *Nano Lett.*, vol. 9, no. 6, pp. 2260–2266, 2009, doi: 10.1021/nl900423g.

[29] Y. Liu, J.-H. Chung, W. K. Liu, and R. S. Ruoff, "Dielectrophoretic assembly of nanowires," *J. Phys. Chem. B*, vol. 110, no. 29, pp. 14098–14106, Jul. 2006, doi: 10.1021/jp061367e.

[30] E. M. Freer, O. Grachev, X. Duan, S. Martin, and D. P. Stumbo, "High-yield self-limiting single-nanowire assembly with dielectrophoresis," *Nature Nanotechnol.*, vol. 5, no. 7, pp. 525–530, 2010, doi: 10.1038/nnano.2010.106.

[31] X. Wang, K. Chen, L. Liu, N. Xiang, and Z. Ni, "Dielectrophoresis-based multi-step nanowire assembly on a flexible superstrate," *Nanotechnology*, vol. 29, no. 2, Jan. 2018, Art. no. 025301, doi: 10.1088/1361-6528/aa9a22.

[32] J. Muster et al., "Electrical transport through individual vanadium pentoxide nanowires," *Adv. Mater.*, vol. 12, no. 6, pp. 420–424, 2000, doi: 10.1002/(SICI)1521-4095(200003)12:6<420::AID-ADMA420>3.0.CO;2-7.

[33] W.-J. Shen, K. W. Sun, and C. S. Lee, "Electrical characterization and Raman spectroscopy of individual vanadium pentoxide nanowire," *J. Nanopart. Res.*, vol. 13, no. 10, pp. 4929–4936, Oct. 2011, doi: 10.1007/s11051-011-0471-3.

[34] A. D. Raj, T. Pazhanivel, P. Suresh Kumar, D. Mangalaraj, D. Nataraj, and N. Ponpandian, "Self assembled V_2O_5 nanorods for gas sensors," *Current Appl. Phys.*, vol. 10, no. 2, pp. 531–537, Mar. 2010, doi: 10.1016/j.cap.2009.07.015.

[35] F. Liu et al., "Polyimide film with low thermal expansion and high transparency by self-enhancement of polyimide/SiC nanofibers net," *RSC Adv.*, vol. 8, no. 34, pp. 19034–19040, 2018, doi: 10.1039/C8RA02479K.

[36] M. Akyurt, G. Zaki, and B. Habeebullah, "Freezing phenomena in ice–water systems," *Energy Convers. Manage.*, vol. 43, no. 14, pp. 1773–1789, 2002, doi: 10.1016/S0196-8904(01)00129-7.

[37] A. Christou, A. S. Dahiya, and R. Dahiya, "Finite element analysis of stress distribution in soft sensors under torsional loading," in *Proc. IEEE Int. Conf. Flexible Printable Sensors Syst. (FLEPS)*, Jul. 2022, pp. 1–4, doi: 10.1109/FLEPS53764.2022.9781555.

João Neto received the integrated master's degrees in micro and nanotechnologies engineering from the NOVA School of Science and Technology (FCT NOVA), Lisbon, in 2019. He is currently pursuing the Ph.D. degree with the Bendable Electronics and Sensing Technologies (BEST) Group, James Watt School of Engineering, University of Glasgow, Glasgow, U.K.

His current research interests encompass flexible and printed electronics, nanowire-based devices, and neuromorphic computing.

Abhishek Singh Dahiya received the Ph.D. degree from the GREMAN Laboratory, Université François Rabelais de Tours, Tours, France, in 2016.

He is currently a Research Associate with the Bendable Electronics and Sensing Technologies (BEST) Group, University of Glasgow, Glasgow, U.K. He has done his post-doctoral research at various CNRS laboratories in France: GREMAN in Tours from 2016 to 2017, ICMCB in Bordeaux from 2018 to 2019, and IES/LIRMM in Montpellier from 2019 to 2020. His current research interests include synthesis of nanomaterials, nanofabrication, energy harvesting, and printed and flexible electronics.

Ravinder Dahiya (Fellow, IEEE) is currently a Professor with the ECE Department, Northeastern University, Boston, MA, USA. He is also the Leader of the Bendable Electronics and Sustainable Technologies (BEST) Research Group [formerly, Bendable Electronics and Sensing Technologies (BEST) Group], University of Glasgow, Glasgow, U.K. His group conducts fundamental and applied research in flexible and printable electronics, tactile sensing, electronic skin, robotics, and wearable systems. He has authored or coauthored about 500 publications, books, and submitted/granted patents and disclosures. He has led several international projects.

Prof. Dahiya was a recipient of the EPSRC Fellowship and Marie Curie and Japanese Monbusho Fellowships. He has received several awards, including 2016 Microelectronic Engineering Young Investigator Award (Elsevier), 2016 Technical Achievement Award from the IEEE Sensors Council, and 12 best paper awards as author or coauthor in international conferences and journal. He is the President of the IEEE Sensors Council from 2022 to 2023. He is the Founding Editor in Chief of IEEE JOURNAL ON FLEXIBLE ELECTRONICS (J-FLEX) and has served on the editorial boards of IEEE SENSORS JOURNAL from 2012 to 2020 and IEEE TRANSACTIONS ON ROBOTICS from 2012 to 2017. He was the Technical Program Co-Chair of the IEEE Sensors 2017 and IEEE Sensors 2018 and also the General Chair or a Co-Chair of several conferences including IEEE International Conference on Flexible and Printable Sensors and Systems (FLEPS) in 2019, 2020, and 2021, which he founded in 2019, and IEEE Sensors 2023.